Magnetic Resonance Spectroscopy with Longitudinal Multispin Orders

S. Sendhil Velan[1,5,*], Kumar Pichumani[2], David Murray[3], Raymond R. Raylman[1,5], Tricia Scott[4], Ayyakannu Manivannan[5] and Larry Halliburton[5]

[1]Center for Advanced Imaging and Department of Radiology, West Virginia University, Morgantown, WV, USA; [2]Department of Chemistry and Biochemistry, Ohio University, Athens, OH, USA; [3]Health Effects Laboratory Division, National Institute for Occupational Safety and Health, 1095 Willowdale Road, M/S 3030, Morgantown, WV, USA; [4]Department of Chemistry, West Virginia University, Morgantown, WV, USA; [5]Department of Physics, West Virginia University, Morgantown, WV, USA

Abstract: Longitudinal multispin orders can be created in spin systems that exhibit scalar, dipolar or quadrupolar couplings. They provide an effective way for measurement of scalar couplings and also to probe molecular interactions and dynamics. They cannot be separated by phase cycling or gradient selection methods which are the only known modes of separating different coherences. In this review we describe the frequency cycling procedure for separating various orders in weakly and strongly coupled spin systems. We provide the analytical solutions that permit determination of the frequency cycle for different spin systems. We also discuss the creation of longitudinal orders through relaxation. Finally we highlight the potential applications including spectral editing, measurement of relative signs of scalar couplings and structural properties of molecules.

Keywords: Magnetic resonance spectroscopy, Frequency cycling, Longitudinal orders, Weak coupling, Strong coupling, Scalar couplings.

1. INTRODUCTION

At thermal equilibrium conditions, longitudinal multispin orders (LOMOs) do not exist. They can be created in spin-systems that exhibit scalar, dipolar or quadrupolar couplings. LOMOs are insensitive to phase cycling or gradient selection methods which are the only known modes of separating different coherences. However the symmetric and antisymmetric longitudinal modes may be distinguished by a π pulse [1]. The symmetric terms are invariant to a π pulse, while the antisymmetric modes change sign:

$$I_{kz} \xrightarrow{\pi(I_{kx})} -I_{kz} \quad (1)$$

$$2I_{kz}I_{lz} \xrightarrow{\pi(I_{kx}+I_{lx})} 2I_{kz}I_{lz} \quad (2)$$

Thus even LOMOs and odd LOMOs can be distinguished by the π pulse. In this review article we discuss two approaches for creating multispin orders. The first approach is by selective inversion of transitions followed by non-selective read pulse employing the frequency cycling (FC) technique [2, 3] to separate various longitudinal orders. Detailed theory for deriving the frequency cycle will be provided for different spin systems. In solution state, LOMOs provide an alternative possibility for visualization of *J* connectivity. We show that they may be employed in various spectroscopic applications like spectral editing, and determination of relative signs of scalar couplings.

The other approach involves creation of multispin orders via the cross-correlated relaxation between different relaxation pathways present for the spin system under study [4]. For example, in a homonuclear AX spin system, there are two main relaxation mechanisms namely dipole-dipole and chemical shift anisotropy (CSA) [5]. Interference terms between these two mechanisms known as "cross-correlations" lead to the creation of longitudinal two spin-order, which can be directly observed by the application of small flip angle detection / mixing pulse or a double quantum filter [5]. Time evolution of the two spin-order created in this way has important structural information such as CSA parameter which is otherwise not possible to be measured in solution phase NMR experiments. Similarly, in a three spin-system, cross-correlated relaxation between different dipolar vectors create longitudinal three spin-order and its time evolution contains the information about the angle subtended by the two dipolar vectors involved. Also, these LOMOs influence the Nuclear Overhauser Effect (NOE) studies, an important tool used in the structure determination of small and biomacromolecules. We discuss the theoretical and experimental details of the creation of LOMOs via different relaxation mechanisms and their applications on determining structural properties of the molecules.

2. PULSE SEQUENCE FOR FREQUENCY CYCLING PROCEDURE TO EDIT LOMO

Fig. (**1**) shows the pulse sequence for separation of various LOMOs by frequency cycling procedure. The pulse sequence incorporates frequency selective inversion by a tailored shaped pulse of appropriate duration and bandwidth, followed by a hard read pulse of fixed phase and flip angle β, phase alternating the receiver on successive scans when the selective inversion frequency is incremented.

*Address correspondence to this author at the Center for Advanced Imaging, Radiology & Physics, West Virginia University, Morgantown, WV-26506, USA; Tel: 304-293-1877; Fax: 304-293-4287;
E-mail: svelan@hsc.wvu.edu

1573-4110/08 $55.00+.00

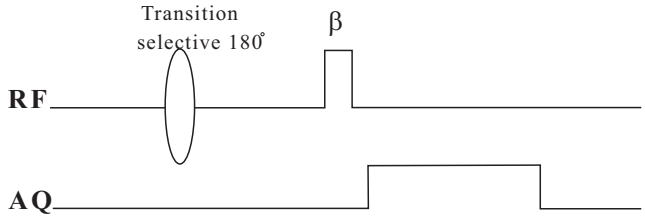

Fig. (1). Pulse sequence for the FC-LOMO experiment. Transition selective 180° pulse followed by a hard (β) pulse. The flip angle (β) should be optimized based on the equation (6). The frequency cycle for the transition selective pulse can be determined using the theoretical expressions for different spin systems.

3. FLIP ANGLE DEPENDENCE OF LOMO

We cannot create observable magnetization by employing a 90° pulse for reconversion of LOMO. The optimal reconversion pulse for *N*-LOMO is order specific.

In the case of 2-LOMO we have :

$$2I_{Kz}I_{Lz} \xrightarrow{\phi\left(I_{Kx}+I_{Lx}\right)} -2\left(I_{Ky}I_{Lz}+I_{Kz}I_{Ly}\right)\sin\phi\cdot\cos\phi \qquad (3)$$

In the case of 3-LOMO we have :

$$4I_{Kz}I_{Lz}I_{Mz} \xrightarrow{\phi\left(I_{Kx}+I_{Lx}+I_{Mx}\right)}$$

$$-4\left(I_{Kz}I_{Lz}I_{My}+I_{Kz}I_{Ly}I_{Mz}+I_{Ky}I_{Lz}I_{Mz}\right)\sin\phi\cdot\cos^2\phi \qquad (4)$$

In general, clearly, the signal available following reconversion of *N*-LOMO is proportional to:

$$S=\sin\phi\cdot\cos^{N-1}\phi \qquad (5)$$

The optimum reconversion pulse flip angle ϕ [2, 3] for N-LOMO can be expressed as:

$$\phi=\sin^{-1}\left[\frac{1}{\sqrt{N}}\right] \qquad (6)$$

4. LOMO SEPARATION IN WEAKLY COUPLED SPIN SYSTEMS

When the frequency separation (chemical shift difference) outweighs by a factor of fifteen or more than the coupling constant involved between the interacting spins then they can be classified under the weak coupling limit.

4.1. AX Spin System

In a weakly coupled two spin-1/2 system AX, the chemical shift difference ($\nu_A - \nu_X$) outweighs by a factor of fifteen or more the coupling constant J_{AX} between the A and X spins.

Fig. (**2**) shows the energy level diagram for the AX spin system. The two A spin transitions and two X spin transitions can be expressed in terms of polarization and shift operators [1].

$$|\alpha\beta\rangle\langle\alpha\alpha| = I_1^{\alpha}I_2^{-} \qquad (7)$$

$$|\beta\beta\rangle\langle\beta\alpha| = I_1^{\beta}I_2^{-} \qquad (8)$$

$$|\beta\alpha\rangle\langle\alpha\alpha| = I_1^{-}I_2^{\alpha} \qquad (9)$$

$$|\beta\beta\rangle\langle\alpha\beta| = I_1^{-}I_2^{\beta} \qquad (10)$$

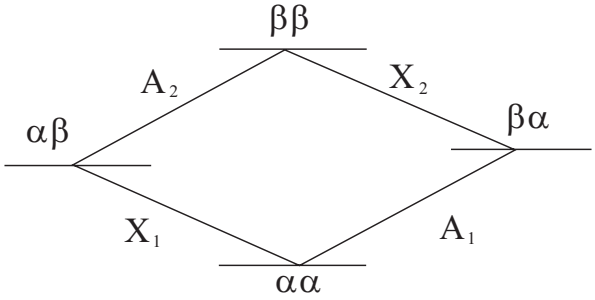

Fig. (2). Energy level diagram for AX spin system.

Considering that the transition selective pulse is going to be of either *x* or *y* phase, and re-expressing the shift operators above in terms of Cartesian components, the effect of the transition selective pulse β on the equilibrium density matrix can be found for the two X spin transitions:

For the X_1 transition we find:

$$\rho_{X_1} = \exp\left\{-i\left(\frac{1}{2}I_{2x}+I_{1z}I_{2x}\right)\beta\right\}\rho_0\exp\left\{i\left(\frac{1}{2}I_{2x}+I_{1z}I_{2x}\right)\beta\right\} \qquad (11)$$

where $\rho_0 = I_{1z}+I_{2z}$ (12)

The resulting density matrix is of the following form for the X_1 spin transition:

$$\rho_{X_1} = -\tfrac{1}{2}I_{2y}\sin\beta - I_{1z}I_{2y}\sin\beta + \tfrac{1}{2}I_{2z}(\cos\beta+1) + I_{1z}I_{2z}(\cos\beta-1) \qquad (13)$$

For the X_2 spin transition we have the pulse operator:

$$\rho_{X_2} = \exp\left\{-i\left(\frac{1}{2}I_{2x}-I_{1z}I_{2x}\right)\beta\right\}\rho_0\exp\left\{i\left(\frac{1}{2}I_{2x}-I_{1z}I_{2x}\right)\beta\right\} \qquad (14)$$

resulting in the following density matrix:

$$\rho_{X_2} = -\tfrac{1}{2}I_{2y}\sin\beta + I_{1z}I_{2y}\sin\beta + \tfrac{1}{2}I_{2z}(\cos\beta+1) - I_{1z}I_{2z}(\cos\beta-1) \qquad (15)$$

These equations exhibit the creation of two-spin order (2-LOMO). The difference between the equations (13) and (15) gives:

$$\rho_{X_1} - \rho_{X_2} = 2I_{1z}I_{2z}(\cos\beta-1) - 2I_{1z}I_{2y}\sin\beta \qquad (16)$$

which reduces, for $\beta=\pi$, to

$$\rho = -4I_{1z}I_{2z} \qquad (17)$$

Similar results can be obtained on considering selective excitation of the A spin transitions. In this two spin-1/2 AX spin system we create 2-LOMO by running the sequence on one of the doublets with the frequency cycle (+1, -2). Here the multiplet components selectively inverted in each scan are labeled from the high-frequency end with successive integers starting from 1, the prefixed sign indicating the receiver acquisition phase. On the other hand, it is possible to systematically expand our procedure outlined above for the two-spin system to achieve discrimination of various LO-

MOs, selectively inverting each line of a multiplet in successive scans, combining with a suitable receiver add/subtract procedure. We term this general procedure as frequency cycling.

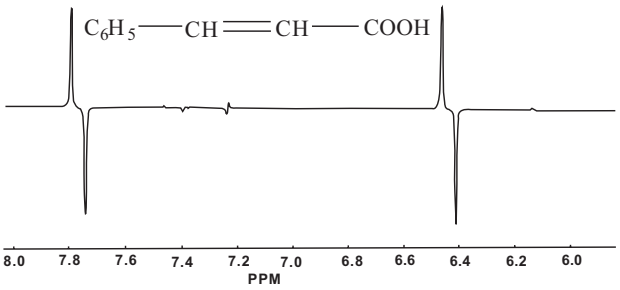

Fig. (3). Separation of 2-LOMO in trans-cinnamic acid using a 300 MHz NMR spectrometer. The experiment was run on the low field doublet with the frequency cycle (+1, –2).

The application of FC-LOMO on cinnamic acid which has an AX spin subsystem is shown in Fig. (**3**). The 2-LOMO spectrum is from the two protons of the CH groups. It clearly suppresses all other resonances arising from the aromatic protons between 7.0 and 7.5 ppm. The experiment was run on the low field doublet with the frequency cycle (+1, –2).

4.2. AMX Spin System

Fig. (**4**) shows the energy level diagram for a non-linear AMX spin system. We can readily see that there are twelve single quantum transitions corresponding to a spectrum of three four-line multiplets for each of the A, M and X spins. The transition selective pulse Hamiltonian of phase x for the each transition can be evaluated using the procedure described for the AX spin system.

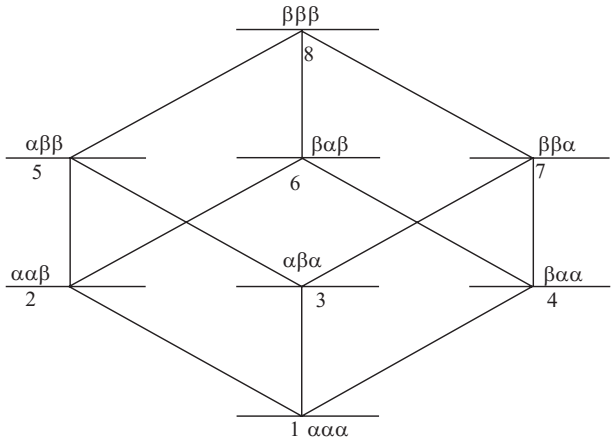

Fig. (4). Energy level diagram for the AMX spin system

We get the following solutions for arbitrary flip angle to the four A spin transitions:

i) $A_z + \frac{1}{4}A_z\{-1+2M_z+2X_z+4M_zX_z\}(\cos\beta-1)$
$-\frac{1}{4}A_y\{1+2M_z+2X_z+4M_zX_z\}(\sin\beta)$ (18)

ii) $A_z - \frac{1}{4}A_z\{-1-2M_z+2X_z+4M_zX_z\}(\cos\beta-1)$
$+\frac{1}{4}A_y\{-1-2M_z+2X_z+4M_zX_z\}(\sin\beta)$ (19)

iii) $A_z - \frac{1}{4}A_z\{-1+2M_z-2X_z+4M_zX_z\}(\cos\beta-1)$
$+\frac{1}{4}A_y\{-1+2M_z-2X_z+4M_zX_z\}(\sin\beta)$ (20)

iv) $A_z - \frac{1}{4}A_z\{-1+2M_z+2X_z-4M_zX_z\}(\cos\beta-1)$
$+\frac{1}{4}A_y\{-1+2M_z+2X_z-4M_zX_z\}(\sin\beta)$ (21)

When $\beta = 180^0$ the solutions take the form:

i) $\frac{1}{2}A_z - A_zM_z - A_zX_z - 2A_zM_zX_z$ (22)

ii) $\frac{1}{2}A_z - A_zM_z + A_zX_z + 2A_zM_zX_z$ (23)

iii) $\frac{1}{2}A_z + A_zM_z - A_zX_z + 2A_zM_zX_z$ (24)

iv) $\frac{1}{2}A_z + A_zM_z + A_zX_z - 2A_zM_zX_z$ (25)

Similar expressions for the M and X spin transition selective pulses with flip angle 180° are given as follows for the M spin transitions:

i) $\frac{1}{2}M_z - M_zX_z - M_zA_z - 2M_zX_zA_z$ (26)

ii) $\frac{1}{2}M_z - M_zX_z + M_zA_z + 2M_zX_zA_z$ (27)

iii) $\frac{1}{2}M_z + M_zX_z - M_zA_z + 2M_zX_zA_z$ (28)

iv) $\frac{1}{2}M_z + M_zX_z + M_zA_z - 2M_zX_zA_z$ (29)

and for the X spin transitions:

i) $\frac{1}{2}X_z - X_zA_z - X_zM_z - 2X_zA_zM_z$ (30)

ii) $\frac{1}{2}X_z - X_zA_z + X_zM_z + 2X_zA_zM_z$ (31)

iii) $\frac{1}{2}X_z + X_zA_z - X_zM_z + 2X_zA_zM_z$ (32)

iv) $\frac{1}{2}X_z + X_zA_z + X_zM_z - 2X_zA_zM_z$ (33)

From the equations (18) to (33) we can readily determine the various frequency cycles for separation of 3- and 2-LOMO. The 3-LOMO can be generated from any one of the A, M, and X spin transitions by running a frequency cycle of (–1, +2, +3, –4) or (+1, –2, –3, +4) from the low field transition to the high field transition. In the case of 2-LOMO separation, AM and AX LOMO can be generated from the A spin transitions, AM and MX 2-LOMO from M spin transitions, and similarly AX and MX 2-LOMO from X spin transitions. From the A spin transitions we can separate the AM 2-LOMO by running a frequency cycle (+1, +2, –3, –4), while by running a frequency cycle of (+1, –2, +3, –4) we can separate the AX 2-LOMO. Similarly, we can apply a frequency cycle of (–1, +2, –3, +4) on the X spin transitions to separate the MX 2-LOMO.

Fig. (**5**) shows the application of FC-LOMO on 2,3-dibromopropionic acid, which constitutes a non-linear AMX spin system. The top trace displays the (MX) 2-LOMO edited spectrum, while the second trace shows the (AM) 2-LOMO edited spectrum. The third trace shows the (AX) 2-LOMO edited spectrum and the fourth trace shows the (AMX) 3-LOMO edited spectrum. The bottom trace shows the one dimensional proton spectrum.

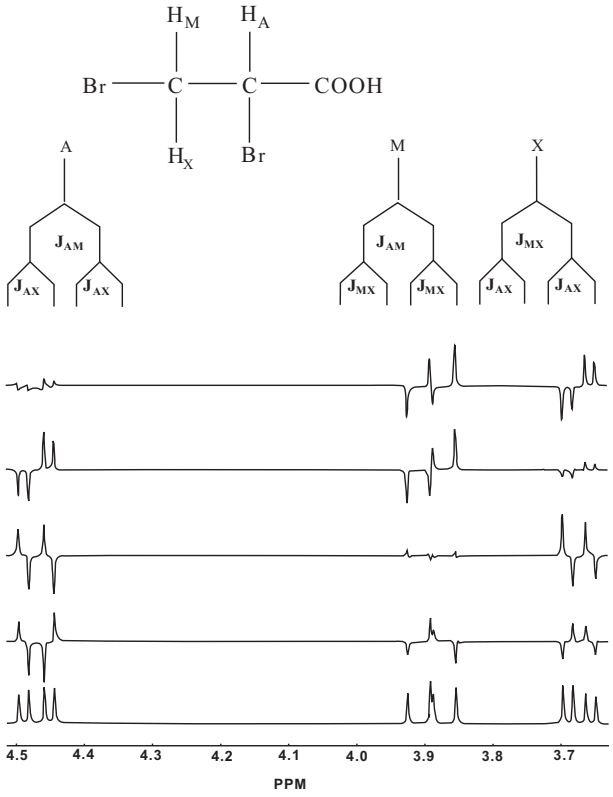

Fig. (5). Application of FC-LOMO procedure for separation of 2 and 3 spin orders in 2,3 dibromopropionic acid (300 MHz). The top trace displays the (MX) 2-LOMO edited spectrum, while the second trace shows the (AM) 2-LOMO edited spectrum. The third trace shows the (AX) 2-LOMO edited spectrum and the fourth trace shows the (AMX) 3-LOMO edited spectrum. The bottom trace shows the one dimensional proton spectrum.

4.3. AX_3 Spin System

The theoretical calculations for the A fragment of the AX_3 spin system are given and the separation of various LOMOs is demonstrated on the lactate and alanine molecules.

Finding the effect of the selective pulse with flip angle β and phase x on the equilibrium density matrix $\rho_0 = A_z + X_{1z} + X_{2z} + X_{3z}$, we get the following solutions for the four A spin transitions:

$$\frac{3}{4}I_z + 2I_z\prod_i S_{iz} + \frac{1}{2}I_z\sum_i S_{iz} - I_z\sum_{i<j}\sum S_{iz}S_{jz} \quad (34)$$

$$\frac{1}{4}I_z - 6I_z\prod_i S_{iz} + \frac{1}{2}I_z\sum_i S_{iz} + I_z\sum_{i<j}\sum S_{iz}S_{jz} \quad (35)$$

$$\frac{1}{4}I_z + 6I_z\prod_i S_{iz} - \frac{1}{2}I_z\sum_i S_{iz} + I_z\sum_{i<j}\sum S_{iz}S_{jz} \quad (36)$$

$$\frac{3}{4}I_z - 2I_z\prod_i S_{iz} - \frac{1}{2}I_z\sum_i S_{iz} - I_z\sum_{i<j}\sum S_{iz}S_{jz} \quad (37)$$

From equations (34) to (37) we can readily see that exclusive 2-LOMO separation can be achieved by running a frequency cycle (+1, −4, +1, −4, +1, −4, +2, −3) on the A quartet. On the other hand, 4–LOMO may be exclusively separated by running a frequency cycle (+1, −2, +3, −4). It may be noted that 3-LOMO in this system is, however, sampled exclusively without any contribution from longitudinal magnetization only if the read pulse is semiselective. Further, in systems with an even number of equivalent spins, the central component of the multiplet of the coupled spin clearly cannot be frequency cycled. Fig. (**6**) shows the application of FC-LOMO separation in sodium lactate. The top and bottom traces show the 2-LOMO and 4-LOMO separation from this molecule.

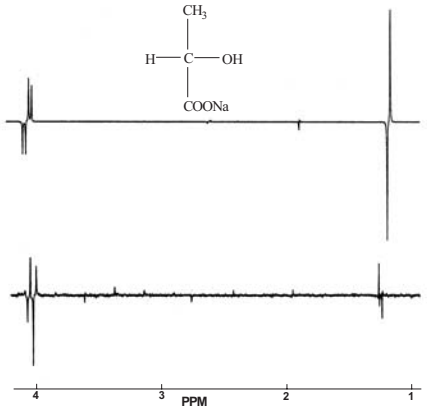

Fig. (6). Application of FC–LOMO on Sodium Lactate (300 MHz). Top trace displays 2–LOMO separation by running the frequency cycle (+1, −4, +1, −4, +1, −4, +2, −3) and the bottom trace displays 4–LOMO separation by running the frequency cycle (+1, −2, +3, −4) on the A quartet.

Fig. (**7**) shows the application of FC-LOMO to alanine. The top trace shows the 2-LOMO edited spectrum and the bottom trace shows the conventional 1D spectrum from this molecule.

5. LONGITUDINAL ORDERS IN STRONGLY COUPLED SPIN SYSTEMS

When the frequency separation (chemical shift difference) outweighs only by a factor of ten or lower than the coupling constant involved between the interacting spins then they can be classified under the strong coupling limit. In this part we show the analytical expressions for AB and ABX spin system. Our goal is to investigate the effect of

strong coupling parameter on various longitudinal orders. The solutions provided here will be of significance for spectral editing sequences using longitudinal orders and also for two-dimensional techniques that involve multispin order pathways.

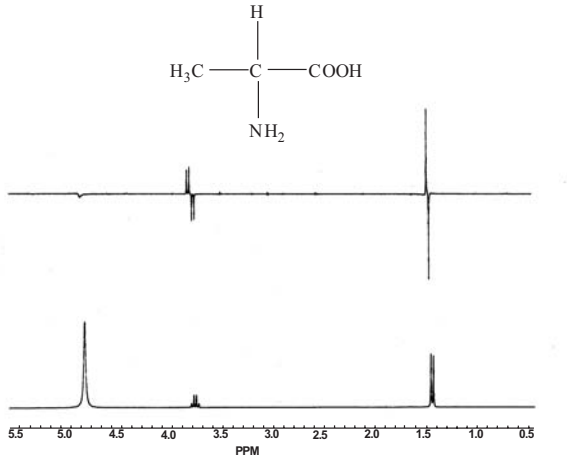

Fig. (7). Application of FC-LOMO on Alanine (300 MHz). Top trace shows the 2-LOMO edited spectrum using same frequency cycle as described in Fig (**6**). The bottom trace the 1D spectrum of Alanine. Note the clear suppression of the water proton signal.

5.1. AB Spin System

In an AB spin system the chemical shift difference (ω_A-ω_B) is comparable with the magnitude of the coupling constant J_{AB} between the A and B spins. The Hamiltonian for strongly coupled AB (spin ½) system can be expressed as

$$H = \omega_1 I_{1z} + \omega_2 I_{2z} + 2\pi J_{12}(I_{1z}I_{2z} + I_{1x}I_{2x} + I_{1y}I_{2y}) \qquad (38)$$

I_{1m} and I_{2m} are the m-components of the nuclear spin angular momentum operators for A and B nuclei; ω_1 and ω_2 are the precession frequencies of A and B nuclei and J_{12} is the scalar coupling constant. A number of biologically important molecules exhibit AB spectral characteristics. For example, citrate which is an important metabolite marker for prostate cancer [6] is an AB spin system. The eigenstates for the AB spin system are $|\alpha\alpha\rangle$, $\cos\theta|\alpha\beta\rangle+\sin\theta|\beta\alpha\rangle$, $\cos\theta|\beta\alpha\rangle-\sin\theta|\alpha\beta\rangle$ and $|\beta\beta\rangle$ where $\theta = \frac{1}{2}\tan^{-1}\left(\frac{2\pi J_{AB}}{\omega_A-\omega_B}\right)$ is the mixing angle. In weak coupling limit the angle θ is very small and the eigenstates will be $|\alpha\alpha\rangle$, $|\alpha\beta\rangle$, $|\beta\alpha\rangle$, $|\beta\beta\rangle$ for the two spin-1/2 system [1,2]. Using similar approach as described for weakly coupled spin systems the solutions for the effect of x phase transition selective pulse with arbitrary flip angle β on the equilibrium density matrix $\rho_0 = I_{1z} + I_{2z}$ is given for the four transitions.

The solutions shown in Equations (39)–(42) provide direct insight into the various terms created for arbitrary flip angles. Using the above expressions Table **1** shows the one spin order, two-spin order and zero quantum coherence's (ZQC) created by a 180° flip angle for all the four transitions.

Fig. (**8**) shows the results from experiments performed on trisodium citrate (AB spin system). Fig. (**8a**) shows the spectrum obtained with a single pulse. The *J* coupling between the two protons involved is 15 Hz and the chemical shift separation between them is 80 Hz clearly indicating a AB spin system. Fig. (**8b**) shows the two-spin order spectrum obtained from the same molecule using the frequency cycling approach. The solutions shown in Table **1** for β = 180° clearly indicate that when a frequency cycle of (+1, –2) or (-1, +2) is run on $|1\rangle\langle 2|, |3\rangle\langle 4|$ or $|1\rangle\langle 3|, |2\rangle\langle 4|$ transitions pure two–spin order can be separated from all other 1–spin order and ZQCs, regardless of the coupling strength. The two-spin order spectrum shown was created with a frequency cycle of (+1, -2) on transitions $|1\rangle\langle 2|, |3\rangle\langle 4|$. The prefixed sign on the frequency cycle indicates the receiver acquisition phase.

In order to verify the solutions for the transition selective pulses on AB spin system to separate the two-spin order theoretical simulations was performed using NMR-SCOPE

$$|1\rangle\langle 2| \Rightarrow I_{1z}\left(\tfrac{1}{2}\sin^2\theta\left(\cos\beta-1\right)+1\right)+I_{1z}I_{2z}\left(\cos\beta-1\right)+I_{2z}\left(\tfrac{1}{2}\cos^2\theta\left(\cos\beta-1\right)+1\right)-I_{1z}I_{2y}\cos\theta\sin\beta$$
$$-I_{1y}\tfrac{1}{2}\sin\theta\sin\beta-I_{2y}\tfrac{1}{2}\cos\theta\sin\beta-\left(I_{1y}I_{2y}+I_{1x}I_{2x}\right)\cos\theta\cdot\sin\theta\left(\cos\beta-1\right)-I_{1y}I_{2z}\sin\theta\sin\beta \qquad (39)$$

$$|3\rangle\langle 4| \Rightarrow I_{1z}\left(\tfrac{1}{2}\sin^2\theta\left(\cos\beta-1\right)+1\right)-I_{1z}I_{2z}\left(\cos\beta-1\right)+I_{2z}\left(\tfrac{1}{2}\cos^2\theta\left(\cos\beta-1\right)+1\right)+I_{1z}I_{2y}\cos\theta\sin\beta$$
$$+\tfrac{1}{2}I_{1y}\sin\theta\sin\beta-\tfrac{1}{2}I_{2y}\cos\theta\sin\beta-\left(I_{1y}I_{2y}+I_{1x}I_{2x}\right)\cos\theta\cdot\sin\theta\left(\cos\beta-1\right)-I_{1y}I_{2z}\sin\theta\sin\beta \qquad (40)$$

$$|3\rangle\langle 1| \Rightarrow I_{1z}\left(\tfrac{1}{2}\cos^2\theta\left(\cos\beta-1\right)+1\right)+I_{1z}I_{2z}\left(\cos\beta-1\right)+I_{2z}\left(\tfrac{1}{2}\sin^2\theta\left(\cos\beta-1\right)+1\right)+I_{1z}I_{2y}\sin\theta\sin\beta$$
$$-I_{1y}\tfrac{1}{2}\cos\theta\sin\beta+I_{2y}\tfrac{1}{2}\sin\theta\sin\beta+\left(I_{1y}I_{2y}+I_{1x}I_{2x}\right)\cos\theta\cdot\sin\theta\left(\cos\beta-1\right)-I_{1y}I_{2z}\cos\theta\sin\beta \qquad (41)$$

$$|4\rangle\langle 2| \Rightarrow I_{1z}\left(\tfrac{1}{2}\cos^2\theta\left(\cos\beta-1\right)+1\right)-I_{1z}I_{2z}\left(\cos\beta-1\right)+I_{2z}\left(\tfrac{1}{2}\sin^2\theta\left(\cos\beta-1\right)+1\right)+I_{1z}I_{2y}\sin\theta\sin\beta$$
$$-\tfrac{1}{2}I_{1y}\cos\theta\sin\beta-\tfrac{1}{2}I_{2y}\sin\theta\sin\beta+\left(I_{1y}I_{2y}+I_{1x}I_{2x}\right)\cos\theta\cdot\sin\theta\left(\cos\beta-1\right)+I_{1y}I_{2z}\cos\theta\sin\beta \qquad (42)$$

Table 1. Longitudinal Orders and ZQC's Created in the Four Transitions in AB Spin System by a x Phase Transition Selective Pulse with a Flip Angle β =180°

	$\|1\rangle\langle 2\|$	$\|3\rangle\langle 4\|$	$\|1\rangle\langle 3\|$	$\|2\rangle\langle 4\|$
1-spin	$-I_{1z}\sin^2\theta + I_{1z}$	$-I_{1z}\sin^2\theta + I_{1z}$	$-I_{1z}\cos^2\theta + I_{1z}$	$-I_{1z}\cos^2\theta + I_{1z}$
order	$-I_{2z}\sin^2\theta + I_{2z}$	$-I_{2z}\sin^2\theta + I_{2z}$	$-I_{2z}\cos^2\theta + I_{2z}$	$-I_{2z}\cos^2\theta + I_{2z}$
2-spin	$-2I_{1z}I_{2z}$	$2I_{1z}I_{2z}$	$-2I_{1z}I_{2z}$	$2I_{1z}I_{2z}$
order				
ZQC	$2(I_{1x}I_{2x} + I_{1y}I_{2y})$ $\sin\theta\times\cos\theta$	$2(I_{1x}I_{2x} + I_{1y}I_{2y})$ $\sin\theta\times\cos\theta$	$-2(I_{1x}I_{2x} + I_{1y}I_{2y})$ $\sin\theta\times\cos\theta$	$-2(I_{1x}I_{2x} + I_{1y}I_{2y})$ $\sin\theta\times\cos\theta$

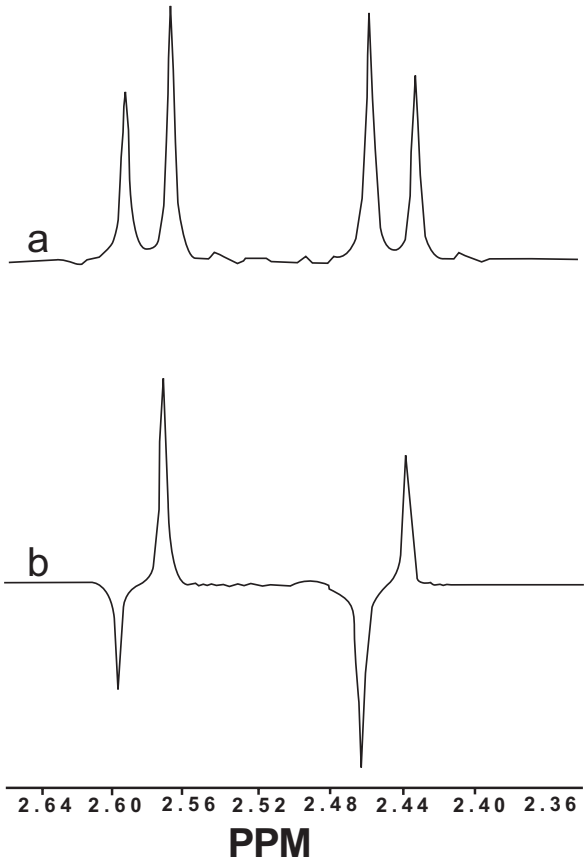

Fig. (8). Application of FC-LOMO on Trisodium citrate (600 MHz). (a) One pulse spectrum of Trisodium citrate obtained with single scan. (b) Two-spin order spectrum of Trisodium citrate obtained with two scans by running a frequency cycle of 1,-2 on the low field doublet.

program [7]. The one pulse experiment was simulated by single hard pulse followed by detection period under strong coupling evolution. The frequency cycling experiment was simulated by transition selective Gaussian pulse followed by an optimum θ° hard pulse. On successive scans the selective inversion frequency was incremented. The strong coupling evolution was employed during the detection period. The receiver phase was determined from the theoretical solutions shown for β = 180° in Table **1**. The simulated spectra of trisodium citrate are shown in Fig. (**9**). Fig. (**9a**) shows the one pulse simulation and Fig. (**9b**) shows two spin order simulation obtained by running the same frequency cycle employed for experimental spectrum. Note the excellent agreement between the experimental and theoretical spectra.

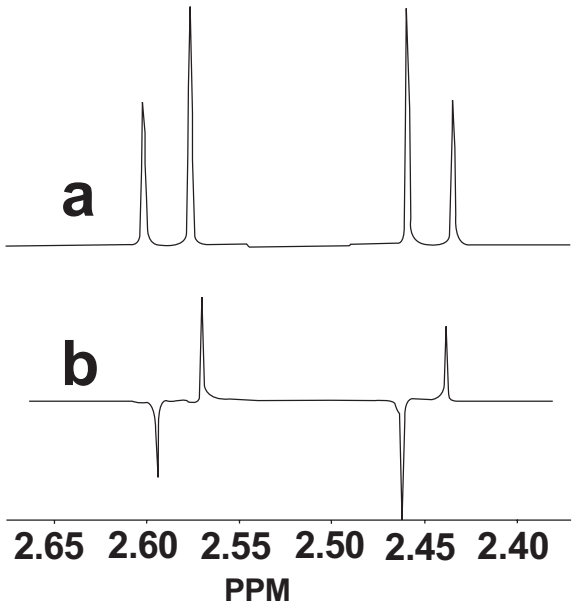

Fig. (9). Simulated spectra of Trisodium citrate (600 MHz). (a) One pulse simulation (b) Two-spin order simulation obtained by running a frequency cycle of 1,-2 on the low field doublet.

5.2. ABX Spin System

When the chemical shift difference between two of the three nuclei (AB) is comparable to their coupling to each other, and both are coupled to a third nucleus (X) with a chemical shift well away from the chemical shifts of other two, the spin system is designated as ABX. Such ABX spectra are common in a number of metabolites, including amino acids present in different tumors. The Hamiltonian for an ABX spin system can be expressed as:

$$H = \omega_1 I_{1z} + \omega_2 I_{2z} + \omega_3 I_{3z} + 2\pi J_{12}(I_{1z}I_{2z} + I_{1x}I_{2x} + I_{1y}I_{2y}) + 2\pi J_{13}(I_{1z}I_{3z}) + 2\pi J_{23}(I_{2z}I_{3z}) \quad (43)$$

where I_{1m}, I_{2m}, I_{3m} are the m-components of the nuclear spin angular momentum operators for A, B and X nuclei; ω_1, ω_2, ω_3 are the precession frequencies of the nuclei A, B, and X respectively. J_{12} indicates the coupling between A and B nuclei and J_{13} is the coupling between A and X nuclei, J_{23} is the coupling between B and X nuclei. The transition-selective Hamiltonian for the ABX transitions can be defined by employing the eight eigenstates shown in the energy level diagram of Fig. (**4**). The two sets of AB sub spectra are defined by the transitions $|1\rangle\langle 4|, |2\rangle\langle 6|, |3\rangle\langle 7|, |5\rangle\langle 8|$ and $|1\rangle\langle 3|$, $|2\rangle\langle 5|$, $|4\rangle\langle 7|$, $|6\rangle\langle 8|$ and the X part of the ABX spectrum is formed by the transitions $|1\rangle\langle 2|, |3\rangle\langle 5|$, $|4\rangle\langle 6|, |7\rangle\langle 8|$ and two combination lines $|3\rangle\langle 6|$ and $|4\rangle\langle 5|$. The combination lines usually appear as outerlines in the high field and low field of the X spin multiplet. They are usually referred to as three spin single quantum coherences as it involves absorption of two quanta with simultaneous emission of one quantum [8]. They are more often weak in intensity and disappear in the weakly coupled AMX spectrum. The x phase transition selective pulse Hamiltonian for all transitions of ABX spin system and the solutions for issuing any arbitrary flip angle on these transitions were derived as described for the AB spin system. Considering the symmetry between the two sets of AB transitions corresponding to X= ± ½ states, it is sufficient to obtain solutions for one set of AB spin transitions.

Table **2** shows the various longitudinal orders and ZQC's created in the following four AB transitions in ABX spin system by a x phase transition selective pulse with a flip angle β =180°. The results indicate that the frequency cycling experiment can be performed in one of the two AB subspectra to separate the AB two spin order from all other longitudinal orders and ZQC's by running a frequency cycle of -1,-2,+3,+4 or +1,+2,-3,-4 from low field transition to high field transition. Similar solutions can be obtained for any arbitrary flip angles for the X-spin transitions $|1\rangle\langle 2|, |3\rangle\langle 5|$, $|4\rangle\langle 6|, |7\rangle\langle 8|$. Table **3** shows the various terms created in the four X spin transitions by a 180° pulse. It is possible to separate the ABX three spin order by running a frequency cycle of -1,+2,+3,-4 or +1,-2,-3,+4 on the X spin transitions $|1\rangle\langle 2|, |3\rangle\langle 5|, |4\rangle\langle 6|, |7\rangle\langle 8|$.

Fig. (**10**) shows the experimental spectra from Styrene dibromide. Fig. (**10a**) shows the ABX part of the spectrum obtained by a single pulse. The chemical shift separation between A and B spins is 30 Hz and the J_{AB} is -11 Hz. The chemical shift separation between A and X nuclei is 673 Hz and between B and X is 643 Hz. The J_{BX} coupling is 10.5 Hz and J_{AX} coupling is 5Hz. Fig. (**10b**) shows the AB two spin order spectrum obtained by running a frequency cycle of -1,-2+3,+4 on the low field AB multiplet where all the four transitions are resolved. Table **2** also indicates that we can separate ABX three spin order by running a frequency cycle of -1,+2,+3,-4 or +1,-2,-3,+4 on one of the AB multiplets. Fig. (**10c**) shows the ABX three spin order spectrum obtained by running a frequency cycle of -1,+2,+3,-4 on the X spin transitions.

Fig. (**11**) shows the simulated spectra of Styrene dibromide. Fig. (**11a**) shows the one pulse simulation and Fig.

Table 2. Longitudinal Orders and ZQC's Created in the Following Four AB Transitions in ABX Spin System by a x Phase Transition Selective Pulse with a Flip Angle β =180°

	$\|1\rangle\langle 4\|$	$\|2\rangle\langle 6\|$	$\|3\rangle\langle 7\|$	$\|5\rangle\langle 8\|$
1-spin	$I_{1z}\left(-\frac{1}{2}\cos^2\theta^+ +1\right)$	$I_{1z}\left(-\frac{1}{2}\cos^2\theta^- +1\right)$	$I_{1z}\left(-\frac{1}{2}\cos^2\theta^+ +1\right)$	$I_{1z}\left(-\frac{1}{2}\cos^2\theta^- +1\right)$
order	$I_{2z}\left(-\frac{1}{2}\sin^2\theta^+ +1\right)$	$I_{2z}\left(-\frac{1}{2}\sin^2\theta^- +1\right)$	$I_{2z}\left(-\frac{1}{2}\sin^2\theta^+ +1\right)$	$I_{2z}\left(-\frac{1}{2}\sin^2\theta^- +1\right)$
2-spin	$-I_{1z}I_{2z}$	$-I_{1z}I_{2z}$	$I_{1z}I_{2z}$	$I_{1z}I_{2z}$
order	$-I_{1z}S_z\cos^2\theta^+$	$I_{1z}S_z\cos^2\theta^-$	$-I_{1z}S_z\cos^2\theta^+$	$I_{1z}S_z\cos^2\theta^-$
	$-I_{2z}S_z\sin^2\theta^+$	$I_{2z}S_z\sin^2\theta^-$	$-I_{2z}S_z\sin^2\theta^+$	$I_{2z}S_z\sin^2\theta^-$
3-spin	$-2I_{1z}I_{2z}S_z$	$2I_{1z}I_{2z}S_z$	$2I_{1z}I_{2z}S_z$	$-2I_{1z}I_{2z}S_z$
order				
ZQC	$-\left(I_{1x}I_{2x}+I_{1y}I_{2y}\right)$ $\sin\theta^+\times\cos\theta^+$	$-\left(I_{1x}I_{2x}+I_{1y}I_{2y}\right)$ $\sin\theta^-\times\cos\theta^-$	$-\left(I_{1x}I_{2x}+I_{1y}I_{2y}\right)$ $\sin\theta^+\times\cos\theta^+$	$-\left(I_{1x}I_{2x}+I_{1y}I_{2y}\right)$ $\sin\theta^-\times\cos\theta^-$
	$-2\left(I_{1x}I_{2x}+I_{1y}I_{2y}\right)S_z$ $\sin\theta^+\times\cos\theta^+$	$2\left(I_{1x}I_{2x}+I_{1y}I_{2y}\right)S_z$ $\sin\theta^-\times\cos\theta^-$	$-2\left(I_{1x}I_{2x}+I_{1y}I_{2y}\right)S_z$ $\sin\theta^+\times\cos\theta^+$	$2\left(I_{1x}I_{2x}+I_{1y}I_{2y}\right)S_z$ $\sin\theta^-\times\cos\theta^-$

Table 3. Longitudinal Orders and ZQC's Created in the Following Four X Spin Transitions of ABX Spin System by a x Phase Transition Selective Pulse with a Flip Angle β =180°

	$\|1\rangle\langle 2\|$	$\|3\rangle\langle 5\|$	$\|4\rangle\langle 6\|$	$\|7\rangle\langle 8\|$
1-spin	$\frac{S_z}{2}$	$\frac{S_z}{2}$	$\frac{S_z}{2}$	$\frac{S_z}{2}$
order		$-I_{1z}+I_{2z}\left[\begin{matrix}-\frac{1}{2}sin\left(\theta^+ +\theta^-\right)\times \\ sin\left(\theta^+ -\theta^-\right)+1\end{matrix}\right]$	$I_{1z}-I_{2z}\left[\begin{matrix}-\frac{1}{2}sin\left(\theta^+ +\theta^-\right)\times \\ sin\left(\theta^+ -\theta^-\right)+1\end{matrix}\right]$	
2-spin	$-I_{1z}S_z$	$-I_{1z}S_z\left(\begin{matrix}cos\left(\theta^+ +\theta^-\right)\times \\ cos\left(\theta^+ -\theta^-\right)\end{matrix}\right)$	$I_{1z}S_z\left(\begin{matrix}cos\left(\theta^+ +\theta^-\right)\times \\ cos\left(\theta^+ -\theta^-\right)\end{matrix}\right)$	$I_{1z}S_z$
order	$-I_{2z}S_z$	$I_{2z}S_z\left(\begin{matrix}cos\left(\theta^+ +\theta^-\right)\times \\ cos\left(\theta^+ -\theta^-\right)\end{matrix}\right)$	$-I_{2z}S_z\left(\begin{matrix}cos\left(\theta^+ +\theta^-\right)\times \\ cos\left(\theta^+ -\theta^-\right)\end{matrix}\right)$	$I_{2z}S_z$
3-spin	$-2I_{1z}I_{2z}S_z$	$2I_{1z}I_{2z}S_z$	$2I_{1z}I_{2z}S_z$	$-2I_{1z}I_{2z}S_z$
order				
ZQC		$-\left(I_{1x}I_{2x}+I_{1y}I_{2y}\right)$ $sin\left(\theta^+ -\theta^-\right)\times cos\left(\theta^+ +\theta^-\right)$	$\left(I_{1x}I_{2x}+I_{1y}I_{2y}\right)$ $sin\left(\theta^+ -\theta^-\right)\times cos\left(\theta^+ +\theta^-\right)$	
		$-2\left(I_{1x}I_{2x}+I_{1y}I_{2y}\right)S_z$ $sin\left(\theta^+ +\theta^-\right)\times cos\left(\theta^+ -\theta^-\right)$	$2\left(I_{1x}I_{2x}+I_{1y}I_{2y}\right)S_z$ $sin\left(\theta^+ +\theta^-\right)\times cos\left(\theta^+ -\theta^-\right)$	

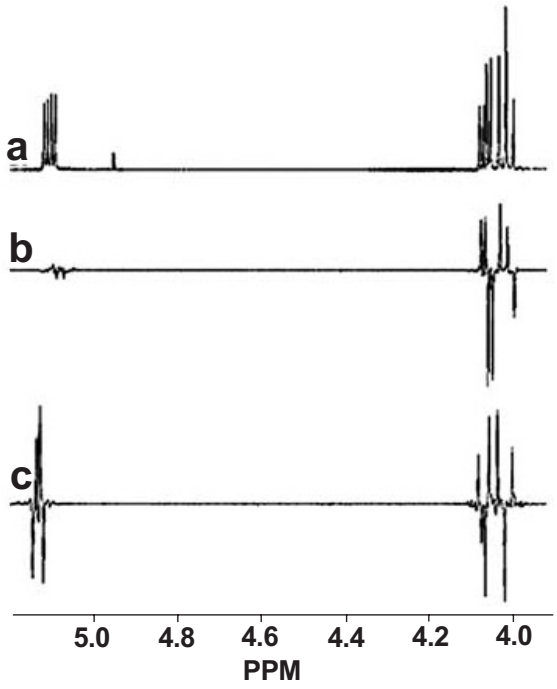

Fig. (10). Application of FC-LOMO to Styrene dibromide (600 MHz). Fig. (**10a**) shows the one pulse spectrum. Fig. (**10b**) shows the AB two spin order spectrum obtained by running a frequency cycle of -1,-2+3,+4 on the low field AB multiplet. Fig. (**10c**) shows the ABX three spin order spectrum obtained by running a frequency cycle of -1,+2,+3,-4 on the X spin transitions.

(**11b**) shows the AB two spin order simulation obtained with same frequency cycle as employed for the experimental spectrum shown in Fig. (**10b**). Note the simulated AB two spin order spectrum resolves the overlapping transition in the high field AB multiplet which is not seen in the experimental spectrum due to the cancellation of the antiphase signal by line broadening. Fig. (**11c**) shows the three spin order simulation obtained by the same frequency cycle employed for experimental spectrum shown in Fig. (**10c**).

From the Tables **2** and **3** it is clear that we cannot separate the AX or BX two spin order independent of the strong coupling parameter. The results indicate that this approach can be employed for separating and analyzing the longitudinal orders in broad range of spin systems that exhibit strong coupling.

6. LONGITUDINAL MULTISPIN ORDER CREATED THROUGH CROSS-CORRELATED NUCLEAR SPIN RELAXATION

Relaxation of a spin after RF perturbation is an important part of NMR spectroscopy as it contains information about the dynamic processes of the molecules. Two important relaxation mechanisms in the case of liquids involving spin ½ nuclei are (a) dipolar relaxation (b) Chemical Shift Anisotropy (CSA) [4]. Let us consider a homonuclear AX spin system which is relaxing by mutual dipolar interaction and CSA relaxation mechanisms of spins A and X. The energy level diagram with the transition probabilities between the eigenstates of AX spin system are shown below in Fig. (**12**).

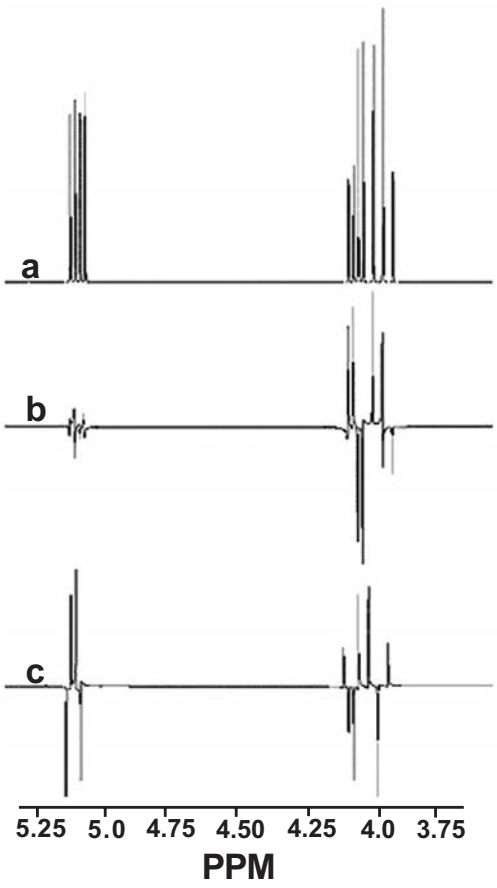

Fig. (11). Simulated FC-LOMO spectra of Styrene dibromide (600 MHz). Fig. (**11a**) shows the one pulse simulation. Fig. (**11b**) shows the AB two spin order simulation obtained with same frequency cycle as employed for the experimental spectrum shown in Fig. (**10b**). Fig. (**11c**) shows the three spin order simulation obtained by the same frequency cycle employed for experimental spectrum shown in Fig. (**10c**).

Zeeman populations of a spin system are given by the master equation:

$$\frac{d}{dt}\Delta\vec{P} = W \quad \Delta\vec{P} \tag{44}$$

Where $\Delta\vec{P}$ = P – P_0 is the column vector of the population deviations from the thermal equilibrium value P_0 and W is the symmetrical relaxation matrix with various transition probabilities. Above master equation in the eigen basis set of the spin Hamiltonian for AX spin system is given as [1, 4, 5]:

where the various transition probabilities are defined as below.

$$\begin{aligned}
W_1^{1A} &= \frac{1}{2}J_{AXAX}(\omega_A) + 2J_{AA}(\omega_A) - 2J_{AX,A}(\omega_A)\\
W_1^{2A} &= \frac{1}{2}J_{AXAX}(\omega_A) + 2J_{AA}(\omega_A) + 2J_{AX,A}(\omega_A)\\
W_1^{1X} &= \frac{1}{2}J_{AXAX}(\omega_X) + 2J_{XX}(\omega_X) - 2J_{AX,A}(\omega_X)\\
W_1^{2X} &= \frac{1}{2}J_{AXAX}(\omega_X) + 2J_{XX}(\omega_X) + 2J_{AX,X}(\omega_X)\\
W_0^{AX} &= \frac{1}{3}J_{AXAX}(\omega_A - \omega_X)\\
W_2^{AX} &= 2J_{AXAX}(\omega_A + \omega_X)
\end{aligned} \tag{46}$$

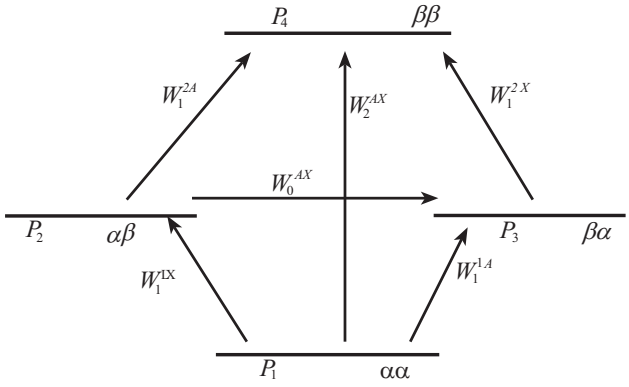

Fig. (12). Energy level diagram of homonuclear AX spin system with the population distribution.

The spectral densities for isotropic reorientation are given by the auto correlation spectral density for dipolar relaxation by spins i and j

$$J_{ijij}(\omega) = \frac{3}{10}\left(\frac{\mu_o}{4\pi}\right)^2 \frac{\gamma_i^2\gamma_j^2\hbar^2}{r_{ij}^6}\frac{\tau_c}{(1+\omega^2\tau_c^2)} \tag{47}$$

for the auto correlation spectral density for CSA relaxation of spin i

$$J_{ii}(\omega) = \frac{1}{30}\gamma_i^2 B_o^2(\Delta\sigma_i)^2 \frac{\tau_c}{(1+\omega^2\tau_c^2)} \tag{48}$$

$$\frac{d}{dt}\begin{pmatrix} P_1 - P_1^0 \\ P_2 - P_2^0 \\ P_3 - P_3^0 \\ P_4 - P_4^0 \end{pmatrix} = \begin{pmatrix} -(W_1^{1A} + W_2^{AX} + W_1^{1X}) & W_1^{1X} & W_1^{1A} & W_2^{AX} \\ W_1^{1X} & -(W_1^{2A} + W_0^{AX} + W_1^{1X}) & W_0^{AX} & W_1^{2A} \\ W_1^{1A} & W_0^{AX} & -(W_1^{1A} + W_0^{AX} + W_1^{2X}) & W_1^{2X} \\ W_2^{AX} & W_1^{2A} & W_1^{2X} & -(W_1^{2A} + W_2^{AX} + W_1^{2X}) \end{pmatrix} \begin{pmatrix} P_1 - P_1^0 \\ P_2 - P_2^0 \\ P_3 - P_3^0 \\ P_4 - P_4^0 \end{pmatrix} \tag{45}$$

for cross correlation spectral density between dipolar interaction between spins i and j and the CSA of spin i

$$J_{iji}(\omega)=\frac{3}{10}\left(\frac{\mu_0}{4\pi}\right)^2\frac{\gamma_i^2\gamma_j\hbar^2}{r_{ij}^3}B_0(\Delta\sigma_i)\frac{1}{2}(3\cos^2\theta_{iji}-1)\frac{\tau_c}{(1+\omega\tau_c^2)} \quad (49)$$

where B_o is the strength of the static magnetic field, γ_i is the gyromagnetic ratio of spin 'i', r_{ij} is internuclear distance between spins 'i' and 'j', $\Delta\sigma_i$ is CSA of spin 'i' and $\theta_{ij,\,i}$ is the angle between the principal axis of the CSA tensor and the internuclear vector r_{ij} . The above relaxation rate equations can also be represented in the basis set of linear operators in Liouville space. In such case, the linear operators are combinations of the populations of the eigen states and are called as "magnetization modes" [9] or "longitudinal spin orders", which are defined for the case of AX two spin system as:

$$\begin{aligned}
\langle \tfrac{1}{2}E\rangle &= \tfrac{1}{2}(P_1+P_2+P_3+P_4)\\
\langle A_z\rangle &= \tfrac{1}{2}(P_1+P_2-P_3-P_4)\\
\langle X_z\rangle &= \tfrac{1}{2}(P_1-P_2+P_3-P_4)\\
\langle 2A_zX_z\rangle &= \tfrac{1}{2}(P_1-P_2-P_3+P_4)
\end{aligned} \quad (50)$$

Where A_z, X_z are the total magnetization of A and X spin respectively which are known as "single spin-order" and $2A_zX_z$ is the two spin-order which corresponds to the differences between the magnetization of the two transitions.

The interconversion of relaxation matrix between the eigenstates and magnetization mode representations is easily done by simple unitary transformation as:

$$\frac{d}{dt}\vec{M}=\Gamma\vec{M} \quad (51)$$

where $\vec{M}$ is the column vector describing the magnetization modes given by

$\vec{M}=\mathrm{V}\ \vec{P}$. Γ is the relaxation matrix in the modes representation given by

$\Gamma=VWV^{-1}$ with V is the transformation matrix which is for a weakly coupled two spin system is given by

$$V=\tfrac{1}{2}\begin{pmatrix}1&1&1&1\\1&1&-1&-1\\1&-1&1&-1\\1&-1&-1&1\end{pmatrix} \quad (52)$$

Rate equation of populations (equation 45) after using the above unitary transform becomes

$$\frac{d}{dt}\begin{pmatrix}\frac{1}{2}E\\A_z\\X_z\\2A_zX_z\end{pmatrix}=\begin{pmatrix}0&0&0&0\\0&\rho_A&\sigma_{AX}&\Delta_{AX}^A\\0&\sigma_{AX}&\rho_X&\Delta_{AX}^X\\0&\Delta_{AX}^A&\Delta_{AX}^X&\rho_{AX}\end{pmatrix}\begin{pmatrix}\frac{1}{2}E\\A_z-A_z^0\\X_z-X_z^0\\2A_zX_z\end{pmatrix} \quad (53)$$

where A_0 and X_0 are the equilibrium values of A and X spin magnetization and the various rate constants in equation (54) are obtained as

$$\begin{aligned}
\rho_A &= -(W_1^{1A}+W_1^{2A}+W_2^{AX}+W_0^{AX})\\
\rho_X &= -(W_1^{1X}+W_1^{2X}+W_2^{AX}+W_0^{AX})\\
\rho_{AX} &= -(W_1^{1A}+W_1^{2A}+W_1^{1X}+W_1^{2X})\\
\sigma_{AX} &= -(W_2^{AX}-W_0^{AX})\\
\Delta_{AX}^A &= -(W_1^{1A}-W_1^{2A})\\
\Delta_{AX}^X &= -(W_1^{1X}-W_1^{2X})
\end{aligned} \quad (54)$$

In equation (53), ρ_A, ρ_X and ρ_{AX} are the self relaxation rates (1/T1) single spin-orders A_z , X_z and two spin-order $2A_zX_z$ respectively. σ_{AX} is the cross relaxation (NOE) between spins A and X whereas Δ_{AX}^A and Δ_{AX}^X are the cross-correlation rates that couple single spin order to two spin-order which solely depends on the dipole-CSA cross correlation spectral density at frequency ω (see equation (46)). Therefore, the amount of longitudinal two spin-order created from single spin-order is directly proportional to the strength of the cross-correlated relaxation interaction which is sensitive to both internuclear distance and Chemical Shift Anisotropy and hence makes the only way to determine the values of geometry dependent Chemical Shift Anisotropy in solution phase with the prior knowledge of internuclear distance and total correlation time.

7. APPLICATIONS WITH LONGITUDINAL MULTI-SPIN ORDERS

7.1. Relative Signs of Couplings

Information on the relative signs of couplings is seldom available from standard high resolution spectra, although in certain systems intensity information may give pointers [10] leading to identification. Generally this can be unraveled by detailed analysis along with special experimental protocols. In particular, double resonance methods (spin tickling) have been employed for determination of the relative sign of couplings [10-15]. The other procedures include sign-labeled polarization transfer (SLAP) [16], and 2D correlation spectroscopy [17-18]. Another procedure [19] involves a fast 2D experiment to determine the relative signs of couplings. Alternatively, the FC–LOMO method offers a straightforward procedure for the determination of relative signs of couplings. As an important example, we discuss below the case of the 3-spin system: by mere inspecting of the LOMO multiplet patterns in the case of simple three-spin-1/2 systems we may readily determine the relative signs of couplings.

Fig. (**13**) shows the application of the FC-LOMO method for determining the relative signs of couplings. When one coupling in a nonlinear three-spin system has a sign opposite to that of the other two, the 3-LOMO multiplets corresponding to both the spins involved in this unique coupling are inverted with respect to the third multiplet as described in the previous section. Bottom trace exhibits the 3-LOMO-edited four-scan spectrum of acrylonitrile. Here all the three multiplets have the same appearance (1, -1, -1, 1). All three couplings therefore have the same sign in this system. The frequency cycle (+1, -2, -3, +4) was employed on the high-field multiplet. Top trace is the 3-LOMO-edited four-scan spec-

trum of vinyl acetate. Note that the low-field multiplet has the appearance (1,-1,-1,1), while the other two multiplets have a (-1,+1,+1,-1) intensity distribution. The geminal coupling between the latter two spins has a sign opposite to that of the other two couplings. The well-resolved low-field multiplet was subject to the frequency cycle (+1, -2, -3, +4).

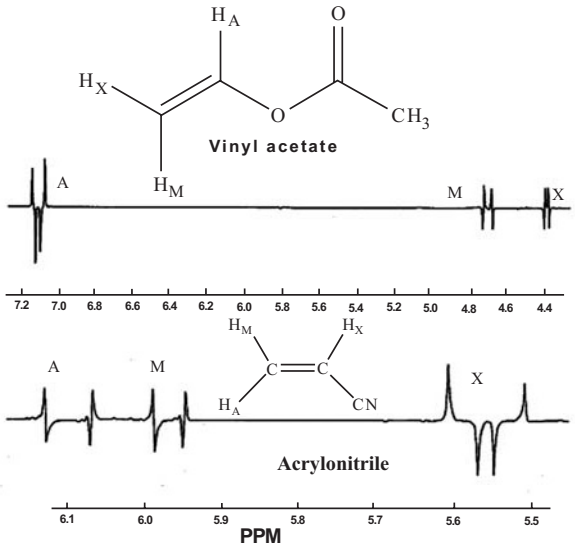

Fig. (13). Determination of relative signs of couplings. Upper trace is the spectrum of vinyl acetate and Lower trace is the spectrum of acrylonitrile. See text for description of the relative signs of couplings.

7.2. Spectral Pattern of Longitudinal Three-Spin Order for Various Sign Combinations

In order to determine the spectral pattern for various sign combinations we show the simulated spectra for weakly and strongly coupled spin systems with various sign combinations. Fig. (**14**) shows the simulations for a weakly coupled AMX spin system at a field strength of 600 MHz with the chemical shifts resonating at 0, 0.6 and 1.2 PPM for A, M, X chemical shifts respectively. The couplings employed were 6, 12 and 22 Hz for J_{AX}, J_{MX} and J_{AM} respectively. Trace (a) shows the simulation of one pulse spectrum and traces (b) – (e) show the various sign combinations. Trace (b) shows the spectrum for J_{AM}, J_{AX}, $J_{MX} > 0$ or J_{AM}, J_{AX}, $J_{MX} < 0$. All the three multiplets have the identical spectral pattern. Trace (c) shows the three-spin order spectrum for J_{AM}, $J_{AX} > 0$, $J_{MX} < 0$ or J_{AM}, $J_{AX} < 0$, $J_{MX} > 0$. Thus the spectral pattern in the multiplets where the coupling J_{MX} has changed sign is reflected by their change in the spectral pattern compared to the A multiplet. Trace (d) shows the three-spin order spectrum for J_{AM}, $J_{MX} > 0$, $J_{AX} < 0$ or J_{AM}, $J_{MX} < 0$ and $J_{AX} > 0$. Trace (e) shows the spectrum for J_{AX}, $J_{MX} > 0$, $J_{AM} < 0$ or J_{AX}, $J_{MX} < 0$, $J_{AM} > 0$.

Similar simulations (Fig. **15**) were performed for a strongly coupled spin system with chemical shifts of 0, 0.2, 1.2 PPM respectively for the A, B and X spins. The couplings were 6, 12 and 22 Hz for J_{AX}, J_{BX} and J_{AB} respectively. The ratio of the chemical shift separation and the J_{AB} is 5.45 corresponding to a strongly coupled case. Trace (a) shows the one pulse spectrum, while traces (b) – (e) show the three-spin order spectra for various sign combinations in the same order as described for the weakly coupled case.

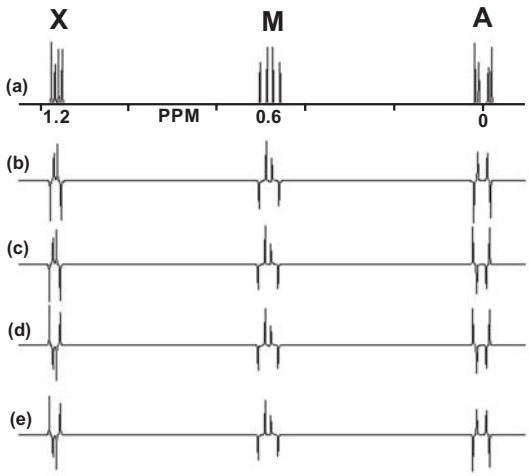

Fig. (14). Simulated spectra of spectral pattern for a weakly coupled AMX spin system (600 MHz) for various sign combinations. See text for description of the relative signs.

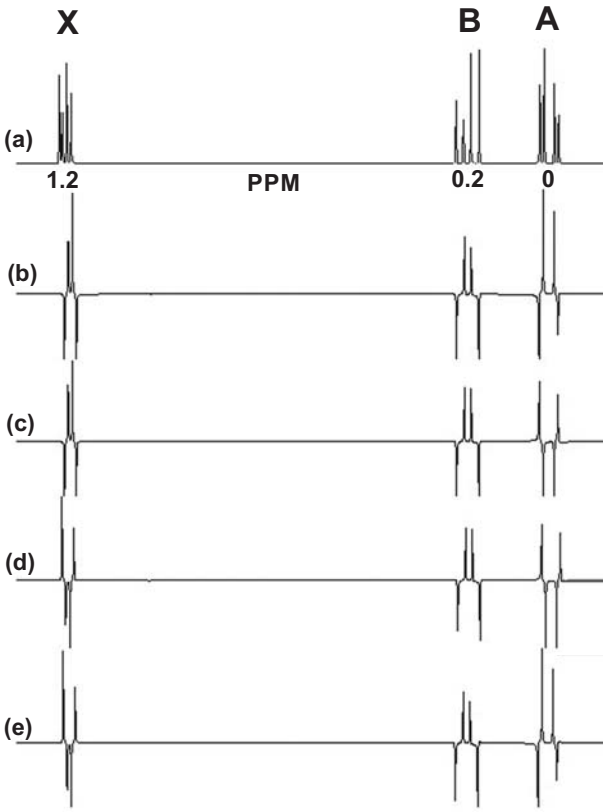

Fig. (15). Simulated spectra of spectral pattern for a strongly coupled ABX spin system (600 MHz) for various sign combinations. See text for description of the relative signs.

Fig. (**16**) shows the experimental three spin-order spectra obtained from a) acrylonitrile b) 2,3 dibromopropionic acid, c) vinyl acetate d) asparagine and e) styrenedibromide. The

three-order order spectrum of acrylonitrile shown in Fig. (**16a**) matches the simulated spectrum shown in Fig. (**14b**) indicating that all the couplings involved in the three multiplets have the same sign. The spectrum of 2,3 dibromopropionic acid shown in Fig. (**16b**) matches with the simulated spectrum shown in Fig. (**14e**) indicating that J_{AM} has changed sign. The spectra from asparagine and styrenedibromide shown in Fig. (**16c**) and Fig. (**16d**) correspond to strongly coupled ABX spin systems. The spectral pattern matched to the simulated spectrum shown in Fig. (**15e**) indicating the sign change for J_{AB}. Note that there is an overlap of two central transitions in the A multiplet of styrene dibromide shown in Fig. (**16e**). Even with the overlap we can clearly identify the spectral pattern for determining the relative sign of couplings. Here again the J_{AB} has changed sign. In general, the sign of a coupling is obtained relative to a known coupling. In the case of larger clusters of coupled spins with spin subsystems, the multispin order edited spectrum may be interpreted with supplementary simulations to determine the relative signs of couplings. Highly complex spectra with increased multiplicity within a multiplet and altered intensity distributions can also be analyzed by this approach.

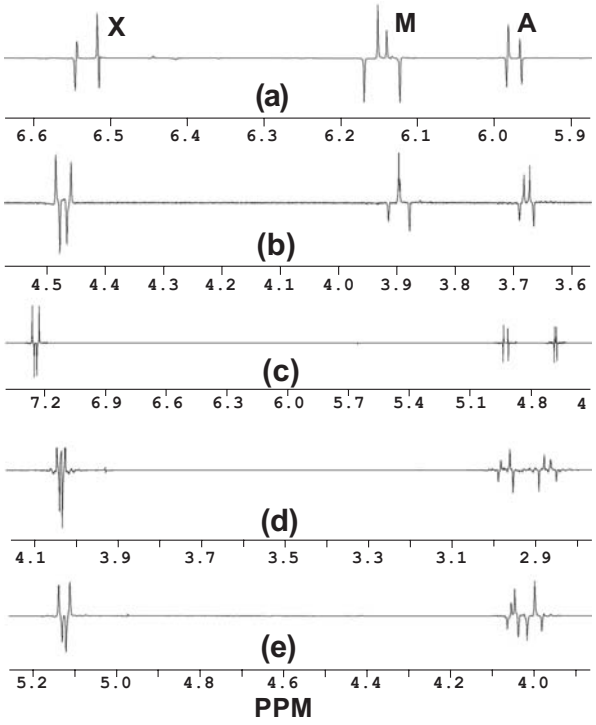

Fig. (16). Experimental three-spin order spectra (600 MHz) of a) Acrylonitrile b) 2,3 dibromopropionic acid c) Vinyl acetate d) Asparagine e) Styrenedibromide

7.3. LOMO studies on glycidyl methacrylate

Glycidyl methacrylate (GMA) is a ten proton system and the LOMO studies on this spin system give information about the relative signs of couplings which is confirmed by simulation studies. Fig. (**17**) shows the application of the FC-LOMO method on this spin system. The bottom trace is the one dimensional spectrum of this molecule and the top trace is the 3-LOMO edited spectrum obtained by running the FC-LOMO with the frequency cycle (+1, -2, -3, +4) on the well resolved multiplet corresponding to the proton 7.

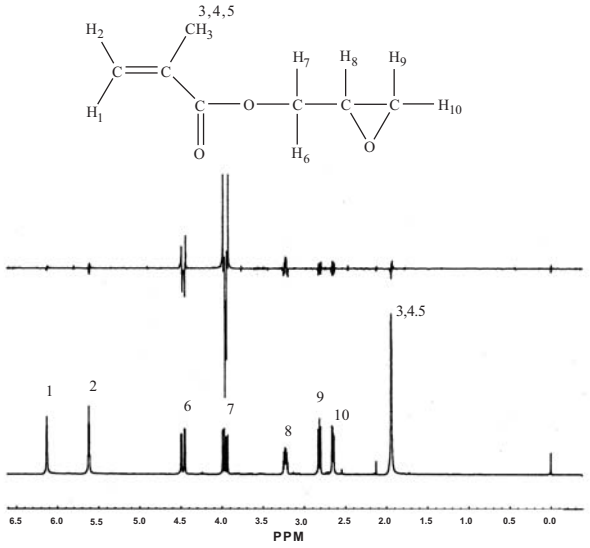

Fig. (17). Application of FC-LOMO on Glycidyl methacrylate (300 MHz). FC-LOMO experiment was performed with the frequency cycle (+1, -2, -3, +4) on the multiplet labeled as proton 7.

Fig. (**18**) shows the expansion plot for the multiplets corresponding to protons 6-10. The bottom trace shows the normal 1D spectrum and the top trace shows the corresponding 3-LOMO spectrum. Only the multiplets corresponding to protons 6, 7, 8 are seen in the 3-LOMO spectrum. The frequency cycle was run on the proton 7 which is the highly resolved multiplet. From the 3-LOMO edited spectrum we can readily see that protons 6, 7 and 8 form an AMX spin system. The LOMO multiplet corresponding to proton 8 is complicated due to the four different couplings it senses, involving protons 6, 7, 9 and 10. In this system, we find from the 1D spectrum the following values of the couplings: $J_{6,8}$ = 2.95 Hz , $J_{7,8}$ = 6.28 Hz and $J_{8,9}$ = 4.23 Hz and $J_{8,10}$ = 2.56 Hz. The couplings were also confirmed by simulations. The simulation is in excellent accord with the experimental spectrum and reveals that J_{67} has the opposite sign with respect to J_{78} and J_{68}.

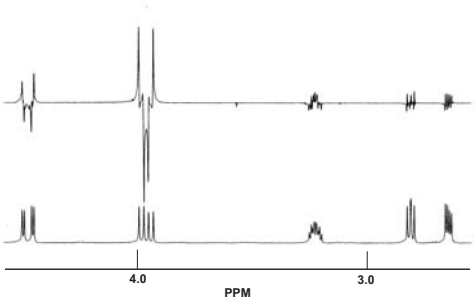

Fig. (18). Expansion plot of Fig. (**17**) showing the protons 6, 7, 8, 9, 10 numbered from low field to high field.

Fig. (**19**) shows the experimental and simulated spectra for proton 8 for confirmation of the various scalar couplings. The upper trace shows the simulated spectrum of proton 8 and the lower trace shows the 1D experimental spectrum. The parameters confirm a weakly coupled system.

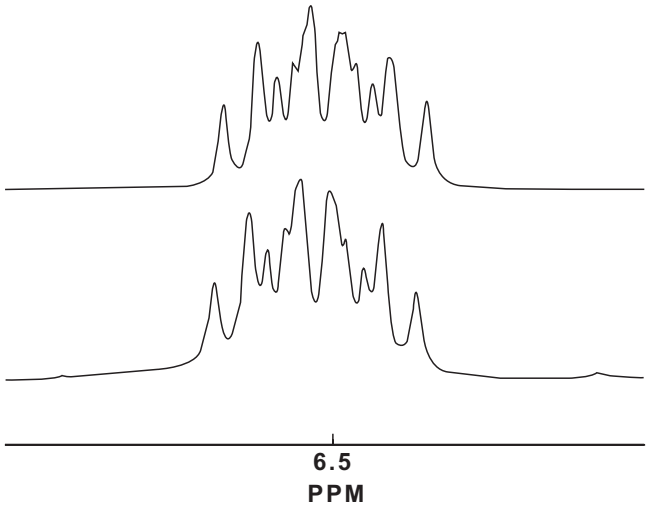

Fig. (19). The upper trace shows the simulated spectrum of proton 8 and the lower trace shows the 1D experimental spectrum.

7.4. Spectral Editing

Spectral editing is another useful application of Longitudinal orders. Earlier studies have shown that metabolites like lactate [20-21] and γ-aminobutyric acid (GABA) [22] can be edited using LOMO. Here we show the frequency cycling procedure for spectral editing using LOMO. In a mixture of spin systems or within a given spin system frequency cycling may be applied on the most highly resolved multiplets to separate the spectra due to distinct spin clusters.

Fig. (**20**) displays the spectral-editing capabilities of FC-LOMO on a 1:16 mixture of trans-cinnamic acid and acrylonitrile. The bottom trace shows the 300 MHz proton spectrum of this mixture. The largest signal was scaled to 3cm. The middle trace shows the 2-LOMO edited spectrum of the sample, selectively inverting each of the low-field cinnamic acid doublet components with the frequency cycle (+1,-2). Suppression of responses from the three-spin system is better than a factor of 60. The largest signal was scaled to 2 cm. The top trace shows the selection of 3-LOMO by application of the frequency cycle (+1, -2, -3, +4) on the high-field acrylonitrile multiplet.

7.5. Determination of Anomeric Configuration Using Dipole-CSA Cross Correlated Relaxation

Recently it was demonstrated that longitudinal cross-correlated relaxation between proton dipolar and Chemical Shift Anisotropy can be used to identify anomeric configuration in ribonucleosides [23]. All the naturally present ribonucleosides are in β anomeric configuration except vitamin B_{12} where a α-ribonucleoside is present as an axial ligand. Also, α-ribonucleosides have other important applications such as antisense and antiviral chemotherapeutic agents and being used in the design of fluorescent probes, which make characterization of their anomeric configuration crucial in understanding their structure and dynamical properties.

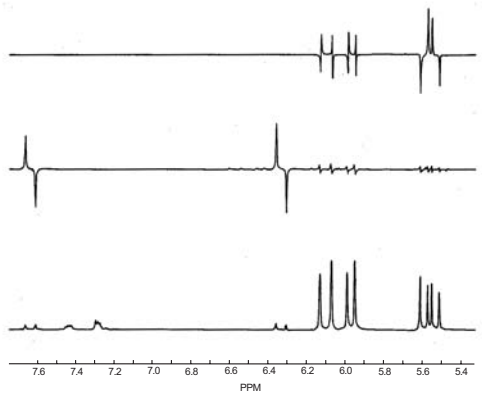

Fig. (20). Spectral Editing in a mixture of trans-cinnamic acid and acrylonitrile**.** See text for details.

Longitudinal cross-correlated relaxation between $\mathbf{H}^{1'}$-$\mathbf{H}^{2'}$ Dipolar and $\mathbf{H}^{1'}$ Chemical Shift Anisotropy (CSA) on three ribonucleosides in both the α and β anomeric configurations whose structures are shown in Fig. (**21**), were studied using standard proton T_1 inversion recovery experiment with a small flip angle detection pulse [24].

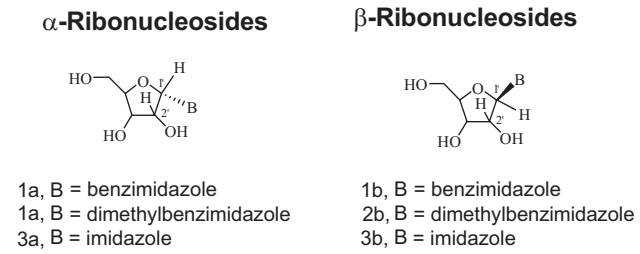

Fig. (21). Schematic representation of α and β ribonucleosides.

During the variable mixing time in this experiment, longitudinal two spin-order between anomeric proton $\mathbf{H}^{1'}$ and $\mathbf{H}^{2'}$ is created due by $\mathbf{H}^{1'}$-$\mathbf{H}^{2'}$ Dipolar and $\mathbf{H}^{1'}$ Chemical Shift Anisotropy (CSA) cross-correlated relaxation and is observed as the differential longitudinal relaxation of each component of the $\mathbf{H}^{1'}$ doublet only by the small flip angle (15°) detection pulse. Use of 90º mixing pulse as used in conventional inversion recovery experiment converts the above two spin-order into non-observable multiple quantum coherences during the acquisition. Difference between the intensities of the doublet is directly proportional to the cross-correlation rate ($\Delta_{1'1'2'}$) by which the two spin order is created due to the $H^{1'}$ CSA and H_1'-H_2' dipolar relaxation mechanisms, and is given by the following expression for the isotropic molecular reorientation (for general expressions, see equation (54)).

$$\Delta_{1'1'2'} = -(1/40)\omega_H D_{1'2'}\left(\Delta\sigma\right)_{1'}^{g}\frac{\tau_c}{(1+\omega^2\tau_c^2)} \qquad (55)$$

where $D_{1'2'} = \left(\frac{\mu_0}{4\pi}\right)^2 \frac{\gamma_H^2}{r_{1'2'}^3}\hbar$ and $\left(\Delta\sigma\right)_{1'} = \frac{1}{2}(3\cos^2\theta - 1)\Delta\sigma_{1'}$

where $r_{1'2'}$ is the internuclear distance between the $H^{1'}$ and $H^{2'}$ protons, θ is the angle between the principal axis of the $H^{1'}$ CSA tensor and $H^{1'}$-$H^{2'}$ internuclear vector, γ_H is the proton gyromagnetic ratio, ω_H is the Larmor frequency of the ^1H nuclear spin and τ_c is the total correlation time of the molecule. $\{\Delta\sigma\}$ is the geometry-dependent Chemical Shift Anisotropy of $H^{1'}$ proton (an axially symmetric CSA tensor is assumed).

The spectra showing the relaxation behavior at different mixing times in the inversion recovery experiment for the $H^{1'}$ proton doublet for the α and β dimethylbenzimidazole are shown in Fig. (**22**). The amount of the $H_z^{1'} H_z^{2'}$ created due to dipole-CSA cross-correlations between $H^{1'}$-$H^{2'}$ and $H^{1'}$ CSA is calculated as described above and results are given below in the Table **4** for the three α and β ribonucleosides shown in Fig. (**21**).

In Table **4**, the $H_{z0}^{1'}$, the equilibrium magnetization of the anomeric proton $H^{1'}$, is calculated as the sum of the intensities of the $H^{1'}$ doublet and the two spin-order is normalized with respect to it. The values of the normalized two spin-order clearly show that there is no effect of dipole-CSA cross-correlations in the ribonucleosides in the β anomeric configuration. The inversion recovery spectra showing the differential relaxation behavior at different mixing times for the $H^{1'}$ proton doublet for the α and β dimethylbenzimidazole are shown in Fig. (**22**). From the above results, it is clear that longitudinal two spin-order created via dipole-CSA relaxation interference terms can be very well used to easily identify anomeric configuration in ribonculeosides.

7.6. Applications of Longitudinal Multispin Orders in NMR Quantum Computing

NMR Spectroscopy is one of the attractive candidates for Quantum Computing due to the fact that nuclear spin coherences have longer decay times. But the main problem with the thermal equilibrium of nuclear spins is that it exists in the statistical superposition of pure spin states whereas quantum computing requires pure states. Recently, there are methods developed to create Pseudo-Pure States which is a sub system within the overall equilibrium density matrix [25-28].

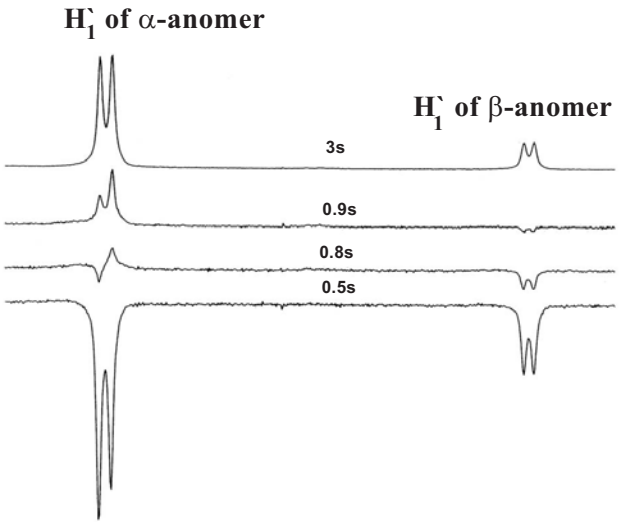

Fig. (22). ^1H inversion recovery spectra of the mixture of 2a and 2b (80% and 20%) for different mixing times. The $H^{1'}$ differential recovery for the α-anomer of 2a indicates the presence of dipole-CSA cross correlations whereas β anomeric proton doublet shows no such effect. $H^{1'}$ chemical shift and $J_{H1'-H2'}$ values of 2a and 2b are 6.48 ppm, 4.95 Hz and 6.13 ppm, 4.24 Hz, respectively.

Consider a spin ½ two spin system AX and its equilibrium density matrix A_z+X_z is given in terms of a matrix representation as:

$$\sigma_{eq} = \tfrac{1}{4} I + \tfrac{\beta}{4} \begin{pmatrix} 1 & 0 & 0 & 0 \\ 0 & 0 & 0 & 0 \\ 0 & 0 & 0 & 0 \\ 0 & 0 & 0 & -1 \end{pmatrix} \qquad (56)$$

where I is the identity operator and $\beta = \dfrac{\hbar\omega_0}{kT}$.

The matrix representation of $A_z+X_z+2A_zX_z$ is given by

Table 4. Maximum Amount of Normalized Proton-Proton Two Spin-Order $H_z^{1'} H_z^{2'}$ Values for the Three Different Ribonucleosides in Both α and β Configuration Shown (Fig. 21)

Ribonucleoside	Anomeric Configuration	$(H_z^{1'} H_z^{2'})/(H_{z0}^{1'})$ *100
1a	α	9.3
1b	β	Not detectable
2a	α	7.06
2b	β	Not detectable
3a	α	5.89
3b	β	Not detectable

$$\sigma_{p-pure} = \begin{pmatrix} 3/2 & 0 & 0 & 0 \\ 0 & -1/2 & 0 & 0 \\ 0 & 0 & -1/2 & 0 \\ 0 & 0 & 0 & -1/2 \end{pmatrix} \quad (57)$$

which can be rewritten as

$$\sigma_{p-pure} = \begin{pmatrix} 2 & 0 & 0 & 0 \\ 0 & 0 & 0 & 0 \\ 0 & 0 & 0 & 0 \\ 0 & 0 & 0 & 0 \end{pmatrix} - \frac{1}{2} I \quad (58)$$

Equation (58) represents a pseudo-pure state which as described is created from the combination of thermal equilibrium (single spin orders) and longitudinal two spin-order. The Unity operator can be ignored as it does not evolve under rf pulses. Therefore creation of various longitudinal multispin orders discussed in this article could well be used in the creation of Pseudo-Pure states which are the important pre-requisites in NMR quantum computation.

CONCLUSIONS

In this review we have provided detailed theoretical solutions for creating longitudinal multispin orders in weakly and strongly coupled spin systems by frequency cycling procedure and also by relaxation. We have also highlighted several applications with LOMO including determination of relative sign of couplings, spectral editing, structural information and quantum computation.

DISCLAIMER

The findings and conclusions in this report are those of the authors and do not necessarily represent the views of the National Institute for Occupational Safety and Health.

ACKNOWLEDGEMENTS

The authors thank the Physics department for support of the 7 Tesla MRI/MRS system and Chemistry department for support of the 14.1Tesla MRS system. We also thank Elsevier and American Chemical Society for permitting us to reproduce material from our earlier work. This research was supported in part by an Internal Health Sciences Center Grant from West Virginia University and NSF Grant 1002165R.

REFERENCES

[1] Ernst, R.R.; Bodenhausen, G.; Wokaun, A. *Principles of nuclear magnetic resonance in one and two dimensions.* Clarendon press: oxford, **1987**.
[2] Chandrakumar, N.; Velan, S.S. *J. Magn. Reson. A*, **1993**, *104*, 363.
[3] Velan, S.S.; *J. Magn. Reson*., **2004**, *171*, 345.
[4] Kumar, A.; Grace, R.C.R.; Madhu, P.K. *Prog. Nucl. Magn. Reson. Spectrosc.*, **2000**, *37*, 191.
[5] Pichumani, K. Cross Correlation studies in relaxation of coupled spins in NMR, Ph.D. Thesis, Indian Institute of Science, Bangalore, India, **1996**.
[6] Costello, L.C.; Franklin, R.B.; Narayan, P. *Prostate*, **1999**, *38*, 237.
[7] Graveron-Demilly, D.; Diop, A.; Briguet, A.; Fenet, B. *J. Magn. Reson. A*, **1993**, *101*, 233.
[8] Freeman, R. *Spin Choreography*, Oxford University Press: New York, **1997**.
[9] Canet, D. *Prog. Nucl. Magn. Reson. Spectrosc.*, **1989**, *21*, 237.
[10] Günther, H. *NMR Spectroscopy*, Second edition, John wiley & Sons, **1995**.
[11] Atta-Ur-Rahman, Nuclear Magnetic Resonance: Basic principles, Springer Verlag, **1986**.
[12] Anderson, W.A.; Freeman, R. *J. Chem. Phys*., **1962**, *37*, 85.
[13] Alexander, S. *J. Chem. Phys*., **1958**, *28*, 358.
[14] Alexander, S. *J. Chem. Phys*., **1960**, *32*, 1700.
[15] Williams, G.A.; Gutowsky, H.S. *J. Chem. Phys*., **1956**, *25*, 1288.
[16] Sørensen, O.W.; Ernst, R.R. *J. Magn. Reson*., **1985**, *63*, 219.
[17] Bax, A.; Freeman, R. *J. Magn. Reson*., **1981**, *44*, 542.
[18] Greisinger, C.; Sørensen, O.W.; Ernst, R.R. *JACS*, **1985**, *107*, 6394.
[19] Chandrakumar, N.; Ramamoorthy, A. *J. Magn. Reson*., **1992**, *99*, 372.
[20] Reddy, R.; Subramanian, V.H.; Clark, B.J.; Leigh, J.S. *Magn. Reson. Med*., **1991**, *19*, 477.
[21] Brereton, I.M.; Rose, S.E.; Galloway, G.J.; Moxon, L.N.; Doddrell, D.M. *Magn. Reson. Med*., **1990**, *16*, 460.
[22] de Graaf, R.A.; Rothman, D.L. *J. Magn. Reson*., **2001**, *152*, 124.
[23] Pichumani, K.; Chandra, T.; Zou, X.; Brown, K.L. *J. Phys. Chem. B*., **2006**, *110*, 5.
[24] Dalvit, C.; Bodenhausen, G. *Chem. Phys. Lett*., **1989**, *161*, 554.
[25] Dorai, K.; Mahesh, T.S.; Arvind, Kumar, A. *Curr. Sci*., **2000**, *79*, 1447.
[26] Gershenfeld, N.; Chuang, I.L. *Science*, **1997**, *275*, 350.
[27] Cory, D.G.; Fahmy, A.F.; Havel, T.F. *Proc. Natl. Acad. Sci. USA*, **1997**, *94*, 1634.
[28] Knill, E.; Chuang, I.L.; Laflamme, R. *Phys. Rev. A*, **1998**, *57*, 3348.

Received: April 24, 2007 Revised: November 12, 2007 Accepted: November 15, 2007